Russian Journal of General Chemistry, Vol. 72, No. 4, 2002, pp. 551–568. Translated from Zhurnal Obshchei Khimii, Vol. 72, No. 4, 2002, pp. 591–610.

Dimensional Effects and Intercluster Interactions in Nanosystems

I. P. Suzdalev

Semenov Institute of Chemical Physics, Russian Academy of Sciences, Moscow, Russia

Received October 24, 2001

Abstract — Magnetic, structural-dynamic, and catalytic properties of nanocluster systems including both isolated and mutually interacting clusters of oxides of iron and other metals were studied. The influence of dimensional effects and intercluster interactions was discovered for nanosystems including metal oxides both with no carrier and in polymeric and carbon matrices. These effects were displayed in decrease in the critical temperature of magnetic phase and structural transitions, appearance of a critical cluster size for first-order magnetic phase transitions, change of the character of magnetic phase transitions, and change of atomic and cluster dynamics, as well as of adsorption and catalytic properties.

INTRODUCTION

According to numerous data of nanometric-scale measurements, matter here acquires new properties as compared both with single atoms and bulk solid. Apart from change in the properties of isolated nanoclusters, special possibilities arise on cluster aggregation to nanostructures or on formation of matrix nanosystems. During the last decade, the development of experimental methods of preparation and investigation of clusters and nanostructures contributed to a significant progress in this field and made possible formulation of the physical chemistry of nanoclusters and nanocluster systems. Herewith, preparative methods are closely related to properties under investigation [1].

This article deals with formation of isolated and interacting nanoclusters in nanosystems and with new properties of the nanosystems related to cluster size effects and intercluster interactions. Nanoclusters and nanostructures were synthesized by the (1) methods of the chemistry of solids and solid-phase chemical reactions and (2) methods of matrix nanostructurization with formation of clusters in micropores by chemical reactions, to proceed from isolated (matrix isolation) clusters to interacting ones [2–13].

Atomic nanocluster dynamics, magnetic properties, magnetic phase transitions, and catalytic properties were investigated as characteristics of clusters and nanosystems. The theoretical methods used included (1) the mathematical model of nucleation in a solid-phase reaction, with accounting for thermodynamic aspects of the process, (2) the thermodynamic model of cluster atomic dynamics, with accounting for cluster interaction, and (3) thermodynamic approaches to description of magnetic phase transitions in nanosystems, with accounting for the surface energy of clusters, defect density, and intercluster interaction.

The experimental techniques included (1) atomic force microscopy, differential thermal analysis, X-ray diffraction analysis, Mössbauer spectroscopy, and Rayleigh scattering of Mössbauer radiation, for characterization of dynamic properties of nanosystems; (2) Mössbauer spectroscopy for measuring cluster size and for investigating magnetic phase transitions and determining critical cluster sizes corresponding to an abrupt change of magnetic properties; (3) the probe method for investigating restricted pore diffusion of clusters to estimate the potentials of cluster movement, and (4) catalytic testing (determination of catalyst activity and selectivity) of the surface and bulk of nanometric layered oxides doped with transition metal ions.

1. FORMATION OF NANOSTRUCTURES. ORGANIZATION AND SELF-ORGANIZATION

Organization of nanoclusters to a nanostructure is an important problem related to creation of new materials with double variation of properties due to cluster size and intercluster interaction. The problem consists in constructing a nanostructure from nanoclusters, like a solid is composed of atoms. Herewith, the notions of "organization" and "selforganization" are rather close to each other, since they make use of the property to clusters to assemble together to form nanostructures similar to atomic structures. Naturally, organization of a nanostructure is based on the same principles and laws as formation of crystals from atoms. However, clusters essentially differ from atoms in that they have a real surface and intercluster and

1070-3632/02/7204-0551 $27.00

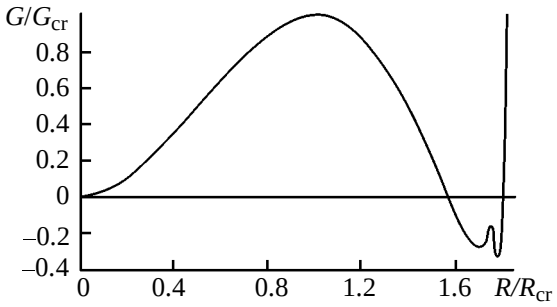

Fig. 1. Gibbs free energy G/G_{cr} of nucleation, growth, and sintering of clusters, calculated by formulas (3) and (4), vs. relative cluster size R/R_{cr}.

interfacial boundaries. These boundaries can be formed by comminution of a solid, for example, with the aid of a mill or of plastic deformation. Formation of nanosystems is accompanied by one more important phenomenon: appearance of a great number of defects and stresses, leading to a cardinal change of the nanosystem properties. All these aspects will be considered in this section.

Nanostructures and nanosystems can be formed of clusters of any types. However, before we consider the formation of nanosystems from solid-phase and matrix clusters, we have to dwell upon the processes of primary cluster nucleation.

a. Nanosystems on the Basis of Solid-Phase Clusters

Solid-phase clusters form in the course of solid-phase chemical reactions, in the process of amorphous-to-crystal phase transitions, by mechanochemical reactions, under high pressure with shear, etc.

In the process of solid-phase chemical reactions, there occurs formation of primary nuclei of the future phase, which then enlarge to nanoclusters and sinter to a massive structure, say, ceramics. Let us consider formation of nanoclusters and nanostructures on the example of thermal decomposition of iron salts. At a temperature above a certain critical or threshold temperature, a labile active reaction medium begins to form, where iron oxide nanoclusters arise [10]. Therewith, cluster growth can be considered as if proceeding in a restricted volume (cell or pore volume) in solution or melt. The reason for that is the diffusion restriction that allows the concentration disturbance of the mother phase, caused by the change in the cluster size, to extend no farther than at the distance $L \sim (Dt)^{1/2}$. Just this distance can be taken for the cluster cell size beyond which components of the mother phase cannot penetrate.

For a system of noncontacting clusters, the dependence of the Gibbs energy of a single cluster ΔG_f on the cluster radius R is determined by formula (1):

$$\Delta G_f = 4\pi R^2\alpha - (4/3)\pi R^3\rho\Delta\mu, \quad (1)$$

where ρ is the density of iron atoms in the cluster, $\Delta\mu$ is the change of the iron chemical potential on passing a single iron atom from the mother phase into the cluster structure, and α is the surface free energy density of the cluster. Let it be N atoms per one cluster in a mixture, including n_0 iron atoms. If $n = (4/3)\pi R^3\rho$ iron atoms of n_0 are located in the cluster structure, then, at $N >> n_0$, we have

$$\Delta\mu = \Delta\mu_0 + \ln[(n_0 - n)/N]. \quad (2)$$

Here $\Delta\mu_0(pT)$ is the change (measured in kT units) of the standard chemical potential of iron on passing a single iron atom into the cluster structure. Clusters do not contact each other on the initial stage. Denoting the cluster volume as $V_f = (4/3)\pi R^3$ and its surface area as $S_f = 4\pi R^2$, we rewrite Eq. (1) as

$$\Delta G_f = \alpha S_f - \{\Delta\mu_0 + \ln[(n_0 - n)/N]\}\rho V_f. \quad (3)$$

The ΔG_f fuction has a maximum at $R = R_{cr}$ and a minimum at $R = R_{max}$ (Fig. 1).

Equation (3) characterizes the stages of nucleation and cluster growth in a system of weakly interacting noncontacting clusters. Further growth of clusters leads to their contact and initiates sintering. The initiation of cluster sintering characterizes a system of strongly interacting clusters. Herewith, if the distance between cluster centers $2R_t$ is constant, the surface area S_s and the volume V_s of a cluster having contacts with k neighbors are sufficiently accurately determined by the expressions

$$S_s = 4\pi R^2 + k2\pi R(R_t - R),$$
$$V_s = (4/3)\pi R^3 + k(1/3)\pi(-2R^3 + 3R^2R_t - R_t^3). \quad (4)$$

Correspondingly, the change of the Gibbs free energy on the sintering stage, when $R > R_t$, is

$$\Delta G = \alpha S_s - \{\Delta\mu_0 + \ln[(n_0 - n)/N]\}\rho V. \quad (5)$$

Thus, the change of the free energy of the system per one cluster is determined by Eq. (3) for $R < R_t$ and by Eq. (5) at $R > R_t$. As an example, Figure 1 represents the $\Delta G(R/R_{cr})$ dependence for $R_t = 1.75R_{cr}$. The dependence in Fig. 1 has three minimuma separated

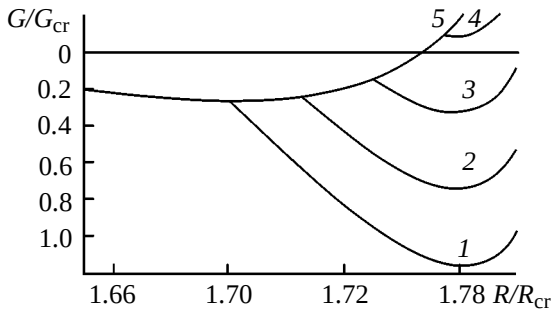

Fig. 2. Gibbs free energy G/G_{cr} in the region of cluster sintering initiation vs. relative cluster size R/R_{cr}, calculated with varied distances between cluster centers R_t: (*1*) $1.7R_{cr}$, (*2*) $1.73R_{cr}$, (*3*) $1.75R_{cr}$, (*4*) $1.77R_{cr}$, and (*5*) $1.8R_{cr}$.

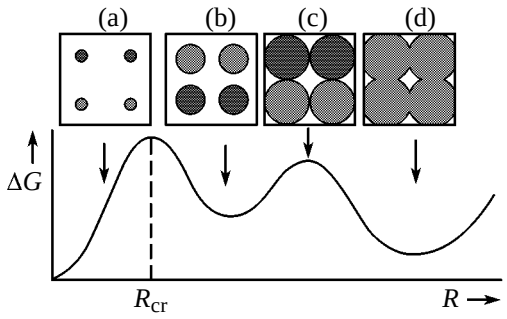

Fig. 3. Scheme of cluster formation, growth, and sintering: (a) nucleation, (b) maximal size of a stable cluster in a weakly interacting system, (c) initiation of sintering, (d) formation of a system of strongly interacting clusters. The arrows relate stages (a)–(d) to the $\Delta G(R)$ curve.

by two maxima. The minimum at $R = 0$ corresponds to the initial state of the mother phase. After passing R_{cr}, the system changes to the first stable state at R = R_{max} and corresponds to an equilibrium state of formed but noncontacting clusters (this is possible if $R_{max} < R_t$). The third minimum corresponds to a system of sintering clusters each having k contacts. Correspondingly, the first maximum at $R = R_{cr}$ forms a nucleation potential barrier, while the second one forms a sintering potential barrier. Figure 2 displays the shape of the sintering potential barrier at $k = 6$ and various R_t values. Sintering proceeds with no barrier at $R_t = 1.7R_{cr}$. Proceeding to sintering at $R_t = 1.75R_{cr}$, i.e. in a system less densely populated with clusters, already requires overcoming a potential barrier. In an even less dense system at $R_t = 1.8R_{cr}$, there is no sintering at all, since it requires increased free energy.

Two minima were obtained in the DTA and TGA curves [10] in the process of thermal decomposition of iron oxalate $Fe_2(C_2O_4)_3 \cdot {}_5H_2O$ at T_d ~200 and 260°C in air. According to data in [10], the first minimum in both the curves corresponds to iron dehydration with CO and CO_2 liberation. Therefore, a labile medium is formed above T_d ~200°C, where nucleation and growth of ferric oxide clusters are possible. The second minimum is probably related to further liberation of CO and CO_2 and to the initiation of sintering of ferric oxide clusters. The cluster size is estimated by the BET procedure and by X-ray diffraction analysis, atomic force microscopy, and Mössbauer spectroscopy. Atomic force microscopy reveals a distinct picture of interacting sintering clusters for the nanocluster system obtained at T_d = 265°C. The agreement between the thermodynamic model of cluster nucleation, growth, and sintering and the experimental data for thermal decomposition of ferric oxalate is shown in Fig. 3. The domain restricted by a dashed line includes four points of initiation of cluster nucleation. The precritical cluster size region ($R < R_{cr}$) corresponding to the stage of fluctuation nucleation with increasing $\Delta G(R)$ function is presented. In the region $R > R_{cr}$, the nucleation process is accompanied by decreasing free energy, proceeds spontaneously, and results in formation of a stable cluster of size R_{max} = 5–6 nm and of a nanosystem of weakly interacting clusters (Fig. 3b). Sintering occurs when the distance between the centers of neighboring clusters ($2R_t$) is sufficiently small. Herewith, if $R_{max} < R_t$, the $\Delta G(R)$ function increases within the region $R_{max} < R < R_t$ and forms the sintering potential barrier with a maximum at $R = R_t$. The potential well corresponding to a strongly interacting system gets shallower with increasing R_t and disappears at $R_t = (R_t)_{max}$. Then sintering becomes impossible because it should be accompanied by increase of the free energy ($\Delta G > 0$). Since R_{max} and R_t are determined by experimental conditions, the result of the topochemical reaction depends on the reactor temperature, on the duration of sintering, and on the sample prehistory. Thus, there are two main stages of nanosystem formation: formation of a nanosystem with weakly interacting clusters (from cluster nucleation to sintering initiation) and formation of a nanosystem with strongly interacting clusters after sintering initiation. The change of the character of cluster interaction changes many properties of the nanosystem; therewith, the development of a strong intercluster interaction and sintering is characterized by significant interfacial stresses. These stresses are generated by the formation of an intermediate neck due to surface tension [14], according to $p = \alpha/x$, where α is the surface tension and x is the neck radius. Setting $\alpha \sim 1$ H/m and $x \sim 1$ nm, we obtain $p \sim 10^9$ Pa. Excess pressure also

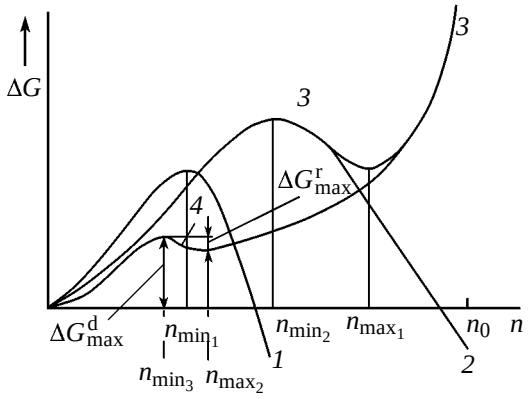

Fig. 4. Function $\Delta G = f(n)$ characterizing growth of a cluster of volume n (*1*) in a supersaturated macrobulk solution, (*2*) in a solution with concentration C, (*3*) in a pore, and (*4*) in a pore [with account for the homogeneity factor $K(\alpha)$].

develops due to the presence of defects and dislocations at the interface and attains 10^9 Pa for clusters of size about 10 nm [1]. The stress or pressure developing in the system of strongly interacting nanoclusters are among the most important factors determining formation of a nanostructure and its properties. Using low-temperature solid-phase reactions and satisfying the conditions for R_t and R_{max}, one can obtain solid-phase nanoclusters of metals, oxides, and chalcogenides.

b. Nanosystems Involving Matrices

Nanoclusters can form in pores and on the surface of adsorbents and porous bodies, such as silicon and aluminium oxides and zeolites, in pores of polymers, ion-exchange resins, and polysorbs, and in porous carbons. Herewith, nanoclusters can be obtained by solid-phase reactions in pores. Solid-phase metal, oxide, and other clusters are also obtained in this way. However, in contrast with the approach described in the preceding section, nanoclusters here may be isolated from each other by the matrix, so that heating of the whole nanosystem does not lead to the significant increase of the cluster size due to sintering. Porous matrices allow nanosystems to be prepared by impregnation with solutions or by performing a chemical reaction in pores as micro- or nanoreactors.

Formation of nanoclusters or nuclei in supercooled liquids and supersaturated solutions in infinite volume was widely investigated and discussed, in the thermodynamic aspect inclusive [15–19] (in [15, 16], the volume finitude was also taken into account). These effects are anyhow related to heterogeneous processes, to interaction of solid and liquid phases, and play an important role not only in crystallization and freezing of a system, but also in many other processes: electrochemistry, adsorption, heterogeneous catalysis, enzymatic reactions, etc. Thermodynamic estimates for the influence of a pore on cluster formation in it were given in [2].

For a supersaturated solution and a supercooled liquid, the Gibbs free energy has an equation [15–19] similar to Eq. (1) for solid-phase reactions. Passing to a solution of concentration

$$C = n_0/N, \tag{6}$$

where n_0 is the number of solute atoms (say, iron), N is the number of solvent atoms, yields

$$\Delta\mu = \Delta\mu_0 + \ln (n_0/N). \tag{7}$$

For a closed pore where a cluster of $n = (4/3)\pi R^3\rho$ atoms forms

$$\Delta\mu = \Delta\mu_0 + \ln [(n_0 - n)/N], \tag{8}$$

where $\Delta\mu_0 = \mu_l - \mu_s$ is the difference between the standard chemical potential in the liquid phase and the chemical potential of the solid. Thus, the Gibbs free energy of a cluster in a closed pore is

$$\Delta G = (4/3)\pi\rho R^3 \left[\frac{3\alpha}{\rho R} - \left(\Delta\mu_0 - \ln \frac{n_0}{n_0 - n} \right) \right], \tag{9}$$

where

$$\Delta\mu = \Delta\mu_0 + \ln (n_0/N). \tag{10}$$

The form of $\Delta G(n)$ is shown in Fig. 4. For infinite volume, curves *1* and *2* have a singularity at the point n_{min}, which corresponds to a critical size of the cluster nuclei. The n_{min} value for a supersaturated solution or a supercooled liquid is determined by Eq. (1). Decrease of the initial concentration n_0/N shifts n_{min_2} toward larger n (curve *2*), since $n_0/N < 1$.

Cluster formation in a closed pore is illustrated by curves *3* and *4*. A shortage of a material (say, of iron atoms) in the solution inside a pore results in that there is a liming size n_{max} beginning with which cluster growth becomes energetically unfavorable. Therefore, further cluster growth in the pore ceases. The second important feature of the pore effect on the formation and growth of clusters is the pore heterogeneity that changes conditions of cluster formation by decreasing the work of formation of the critical cluster [2]. Estimations by Eq. (9) give the following results.

(1) For the region where $n << n_0$

$$n_{min} = 32\alpha^3/3\rho^2\Delta\mu_0^3. \quad (11)$$

It immediately follows from Eq. (11) that the critical cluster size decreases [see Eq. (10)] with increasing concentration C. Herewith, the height of the energetic barrier for the formation of a stable cluster is

$$\Delta G_{max} = 16\pi\alpha^3/3\rho^2\Delta\mu_0^2. \quad (12)$$

(2) In the region where $n >> n_{min}$ ($\Delta\mu > 2\alpha/\rho R$) and $n < n_0$

$$n_{max} = n_0 \frac{\Delta\mu_0}{2 + \Delta\mu_0}. \quad (13)$$

Thus, the maximum cluster size in a pore n_{max} is always smaller than n_0 and increases with pore size at a given concentration. At estimating n_{max}, one should, however, account for the heterogeneity effect diminishing n_{max}, as well as for the following fact. As the pore size increases in the range 10–100 nm and more, the probability increases of formation of several clusters in one pore, which naturally leads to decrease in nmax and to the condition $n_{max} << n_0$ for large pores.

Heterogeneity decreases the energy barrier for cluster formation with. Herewith, one can consider ΔG^r_{max} both for the formation, ΔG^d_{max}, and for the reverse disintegration, ΔG^r_{max}, of clusters. With the heterogeneity factor $K < 1$

$$\Delta G^d_{max} = 16\pi\alpha^3 K/3\rho^2\Delta\mu_0^2, \quad (14)$$

and the pore effect decreases ΔG^r_{max}. As a result, $\Delta G^r_{max} < \Delta G^d_{max}$ at decreasing n_{max} (especially for pores of ~10 nm). The surface and volume of the pore, too, accelerate cluster formation by lowering the energy barrier and the heterogeneity factor [2, 19].

Formation of ferric hydroxide clusters was investigated in organic sorbents, copolymers of styrene and divinylbenzene (polysorbs), with specific surface areas up to hundreds m^2/g and the pore size from 7 to 50–100 nm [2, 4]. The surface of polysorbs does not contain functional groups, so the influence of chemisorption on the cluster formation was not considered. Such a nanosystem makes possible consideration of ferric hydroxide clusters weakly interacting with each other and with the matrix. Polysorbs were impregnated with ferric chloride solutions of various concentrations and blown with air containing an ammonia admixture (0.08–0.008%). As a consequence, the irreversible chemical reaction

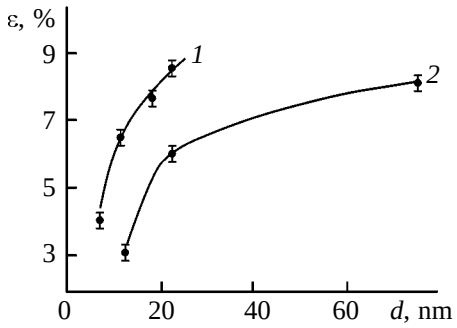

Fig. 5. Intensity of Mössbauer spectral lines vs. pore diameter d (T = 300 K) at ammonia concentrations in the air of (*1*) 0.08 and (*2*) 0.008%.

$$FeCl_3 \cdot 6H_2O + NH_3 \longrightarrow Fe(OH)_3 + NH_4Cl + NH_4OH$$

took place in a pore, and single molecules of ferric hydroxide formed. This changed the pH of the medium and caused growth of insoluble ferric hydroxide clusters in the pore. Changes of the spectral intensity ε of Mössbauer spectra for ferric hydroxide clusters in pores of various sizes at varied ammonia concentration in the air [2] (Fig. 5). Decreasing pore size corresponds to decreasing cluster size, as it follows, for example, from Eq. (13). Thus, it was found that the spectrum line intensities ε decrease with cluster size. Besides, ε for large pores decreased with increasing iron concentration, which can be explained by formation of several clusters of smaller sizes in one pore. A sig-nificant increase of the cluster formation rate in a pore as compared with a macrovolume was also noted, in accordance with Eq. (14) and the heterogeneity factor.

One more active nanosystem-forming matrix is porous charcoal. The deposition of metal salts, such as ferric oxalate $Fe_2(C_2O_4)_3 \cdot 5H_2O$, followed by calcination and reduction in a hydrogen atmosphere, result in formation of a mixed heterogeneous system of Fe_3O_4, γ-Fe_2O_3, and metallic iron clusters on the carbon support. The oxide clusters were 7 to 12 nm in size and the iron (α-Fe) clusters, 7 to 3 nm, depending on the hydrogen reduction time [7]. It is of note that the nanosystem possesses a self-formation property. Hydrogenization (burning out of carbon) occurs in the course of hydrogen reduction. This can be accompanied by increasing pore size. The nature of the carbon surface strongly affects the size and composition of clusters [20, 21].

2. PROPERTIES OF NANOCLUSTER SYSTEMS

As was already noted in Section 1, isolated nanoclusters possess unique properties due to their size.

However, observation of the properties of an isolated nanocluster is often not a less challenging problem that cluster preparation. Nanoclusters mostly occur in the state of interaction with each other, which not only can change the properties of isolated nanoclusters, but also can endow them with new properties. Herewith, the existence of cluster organization and self-organization facilitates calculation and prediction of the properties of nanocluster systems. As characteristic properties of nanosystems, atomic cluster dynamics and magnetic phase transitions are considered in this section, with account for intercluster interactions. Atomic and cluster mobility determines optical, thermodynamic, adsorption, and some other properties of nanosystems. It is worthy to consider intracluster atomic dynamics and possible intercluster mobility in a nanosystem where a cluster moves as a whole.

a. Intracluster Atomic Dynamics

Intracluster atomic mobility (in melting dynamics as example) is studied by microscopy and quantum statistics, as well as methods based on thermodynamic models and computer (molecular dynamics or Monte Carlo) simulation.

Change in the thermodynamic state of a cluster can be described by the free energy $\Delta F = \Delta E - T\Delta S$, where E is the internal energy of the cluster and S is entropy. As is known, $S = -kT\ln Z$ ($Z = \Sigma g_i \exp(E_i/kT)$ is the state distribution function, where g_i and E_i are degeneracy and the energy of the ith level). Many publications (see, e.g., [22, 23]) are devoted to calculation of Z with the aid of quantum-statistical methods. The energy distribution of a solid cluster is essentially different from that characteristic of the liquid state. As compared with liquid, the state density for the solid state is higher at low energies and lower at high temperatures. As a result, the temperature of the equilibrium transition from the solid to liquid state, T_{eq}, appears. The energy change ΔE is determined by vibrational and rotational energy levels of the solid. The free energy of the cluster increases with temperature. However, due to the high state density of liquids, the determining role belongs to the entropy factor, i.e. the disorder of motions characteristic of liquids. The way of calculation of T_{eq} or the melting point of the cluster, depends on the state model for the solid and liquid and is also determined by the state number, i.e. by the cluster size. The presence of both solid and liquid states is possible if clusters are in equilibrium ($T = T_{eq}$).

Cluster melting can be considered in terms of thermodynamic approaches [3, 5]. In the course of solid-phase reactions or cluster formation from solutions and melts, the state of the cluster is determined by its Gibbs energy $G = f(\alpha, \mu, R)$. The difference of the Gibbs energies of the cluster in the liquid and solid states is

$$\Delta G = 4\pi R^2 \Delta\alpha + (4/3)\pi R^3 \rho \Delta\mu, \quad (15)$$

where $\Delta\alpha = \alpha_l - \alpha_s$ is the difference in the specific surface free energies, $\Delta\mu = \mu_l - \mu_s$ is the chemical potential difference for the liquid and solid states of the cluster. The quantity $(4/3)\pi R^3\rho$ is assumed to be unchanged.[1] Evidently, for melting we have $\Delta a < 0$ and $\Delta\mu > 0$.[2] The $\Delta G(R)$ dependence is represented in Fig. 6. The critical cluster size at $\Delta G = 0$ is

$$R_{cr} = -3\Delta\alpha/\rho\Delta\mu, \quad (16)$$

and the cluster is in the liquid state at $R < R_{cr}$. Equation (16) shows that the solid–liquid state is impossible if $\Delta\alpha = 0$, i.e. for single atoms in a matrix, when the cluster has not yet formed. At the same time, $\Delta\alpha$ seems to be a quantity which is maximal for a free cluster. Any intercluster interaction decreases this quantity and also the quantity R_{cr} that determines the range of possible fluctuations of the solid and liquid states. The cluster stability can be characterized by the pressure change $\delta P = P_0 - P$ or by the temperature change $\delta T = T_0 - T$ which correspond to the chemical potential difference $\Delta\mu = f(P, T)$ and draw the phases to equilibrium at a given cluster size (P_0 and T_0 are the medium pressure and the temperature of bulk body, respectively).

We replace $\Delta\mu$ by its expansion in powers of ΔP at the point P_0. We also account for the relations $\delta\mu_l/\delta P = V_l$ and $\delta\mu_s/\delta P = V_s$ [24] where V_l and V_s are the molecular volumes of the cluster in the liquid and solid states, respectively, to obtain

$$\Delta\mu \approx -(V_l - V_s)\delta P. \quad (17)$$

The variables T and P are not independent in this case because of the phase equilibrium condition [Eq. (16)]. Therefore, we use the Clapeyron–Clausius equation $\delta P = qdT/T_0(V_l - V_s)$, where q is the latent heat of phase transition. This yields[3]

$$\Delta\mu \approx -qdT/T_0. \quad (18)$$

---

[1] This means that the quantities R and ρ, different for different phases, can be simultaneously related to either phase (hereinafter, comments of A.I. Rusanov).

[2] The latter is true below the melting point of bulk sample.

[3] Equation (18) immediately follows from the thermodynamic relationship $d\mu = -sdT$ (s is molecular entropy) and does not require the Clapeyron–Clausius equation.

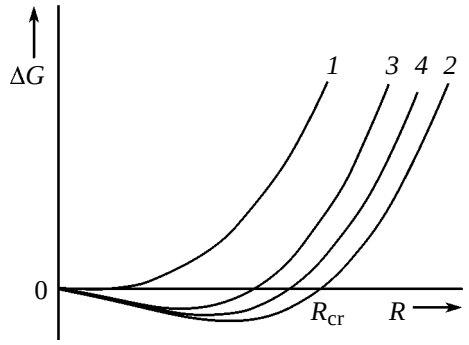

Fig. 6. Gibbs free energy of a cluster in the solid and liquid state vs. cluster size for (*1*) single atom or fragment (α = 0), (*2*) isolated cluster, (*3*) interacting clusters, and (*4*) clusters treated with surfactants.

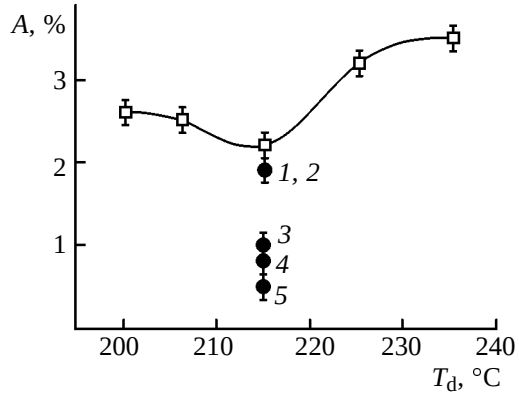

Fig. 7. Mössbauer spectral area at T = 300 K for ferric oxide clusters vs. the temperature of thermal decomposition T_d of (light symbols) ferric oxalate. (Dark symbols) Treatment with (*1*) ethanol, (*2*) isopropanol, (*3*) Twin-65, (*4*) butanol, and (*5*) sodium dodecyl sulfate.

Putting Eq. (18) in Eq. (16) results in a hyperbolic dependence of the temperature of the phase transition in the cluster on its radius:

$$\delta T/T_0 \approx -3\Delta\alpha/\rho qR. \quad (19)$$

The dependence given by Eq. (15) and represented in Fig. 6 leads to a conclusion that, at given temperature and pressure, the initially stable cluster structure ($\Delta\mu > 0$) becomes metastable with respect to the liquid phase when $R < R_{cr}$. In addition, the dependence given by Eq. (15) shows that the melting point decreases with decreasing cluster size.

Analysis of experimental data on the atomic dynamics of clusters gives evidence to suggest mostly increased rms displacements in metal and oxide [25]. In W, β-Sn, Fe, and α-Fe_2O_3It clusters, decreasing probability of the Mössbauer effect *fa* (and increasing displacement $<r^2>$) was observed. An exception are Au clusters 6–20 nm in size, where *fa* increased and $<r^2>$ decreased with decreasing cluster size. This effect is accredited to the long-wave restriction of the phonon spectrum. Increased $<r^2>$ were also revealed for thin oxide films on the surface of β-Sn and Fe clusters. Along with increased $<r^2>$, surface anisotropy might be an important property of atomic dynamics. Such an anisotropy of atomic oscillations, along and across the surface, was observed for iron and tin atoms on the developed surface of η-Al_2O_3, silica gels, and zeolites.

Decreasing melting point down to room temperature was observed in gold and tin nanoclusters [1]. For tin, the separation of melting and freezing points and a peculiar solid–liquid state possessing higher intracluster mobility in the intermediate temperature range were revealed [1]. The results in [2, 5] for ferric oxide nanoclusters are interpreted in terms of increased rms displacements and melting points. Figures 5 and 7 display the Fe Mössbauer spectral data for ferric hydroxide clusters in polysorbs with the pore diameter decreasing from 7.5 and 0.75 nm and for the ferric oxide nanosystem obtained by thermal decomposition of ferric salts, respectively. As was already noted, a strong decrease in the intensity (area) of spectral line with pore size was observed for ferric hydroxide clusters in polysorb pores (Fig. 5). According to the nucleation conditions [Eqs. (2) and (5)], decreasing pore size decreases the cluster size in the pore. The dependence in Fig. 5 looks as related to the onset of cluster melting, which is associated with increasing intracluster atomic mobility. For γ-ferric oxide clusters, the dependence of spectral area A on the temperature T_d of thermal decomposition of ferric oxalate has a minimum at T ~215°C (Fig. 7). The quantity T_d is related to the average cluster size, estimated from Mössbauer spectral data and by calculations using the superparamagnetic relaxation time $\tau = \tau_0 \exp(KV/kT)$ with $\tau_0 = 10^{-9}$ s and $K = 2 \times 10^5$ J/m^3, where K is the magnetic anisotropy constant and V is the cluster volume. It was found that the cluster size increases with temperature from d ~2 nm at T_d = 215°C to d ~4 nm at T_d = 235°C. Thus, the right-hand branch of the curve in Fig. 7 is associated with decreasing quantity A and increasing atomic mobility, as with iron hydroxide clusters in polysorb pores. Notably, there is no motion of a cluster as a whole in ferric hydroxide and oxide clusters, as judged from the fact that the spectra lack the "broad spectral component" related to restricted diffusion of clusters

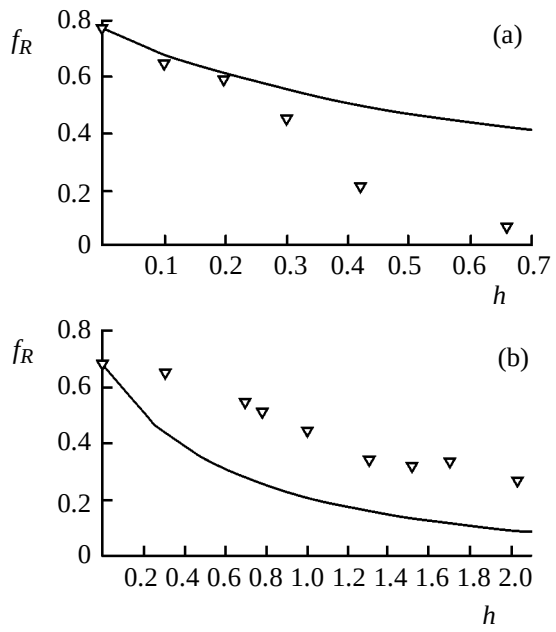

Fig. 8. Integral elastic fraction of Rayleigh scattering of Mössbauer radiation f_R vs. water/polymer weigh ratio h for (a) SGK-7 acrylate cationite (2%) [(dots) experiment and (solid line) calculation under the assumption that $f_R(H_2O) = 0$, $f_R(p) = 0.77 = \text{const}$] and (b) Porolas TM polymeric sorbent [(dots) experiment and (solid line) calculation under assumption that $f_R(H_2O) = 0$, $f_R(p) = 0.67 = \text{const}$].

in pores (this topic will be discussed in the section dealing with intercluster dynamics). Therefore, changes in spectral area are related to intracluster mobility.

The left, ascending branch of the dependence is related to further decrease in T_d and, correspondingly, in cluster size. In fact, this leads to disappearance of clusters and appearance of single atoms, dimers, and trimers of Fe^{3+} as nuclei of γ-ferric oxide clusters (cf. Fig. 6 for $\Delta\alpha = 0$). Thus, the minimum in the dependence $A = f(T_d)$ at $T_d = 215°C$ can be assigned to the onset of formation ferric oxide clusters.

As was already noted above, intercluster interactions should strongly affect atomic cluster mobility. This results in decreased surface energy (quantity $\Delta\alpha$, Fig. 6). Intercluster interactions and stresses can be abated by treatment with surfactants in combination with mechanical treatment. Upon the action of surfactants, the spectral area considerably diminished (Fig. 7). Thus, abating intercluster interactions increases intracluster atomic mobility and lowers melting point. Equation (16) allows one to estimate the R_{cr} value for melting of γ-ferric oxide clusters and to compare it with the $R(V)$ value observed in the Mössbauer spectra. Using for Fe_2O_3 $\rho = 5.18 \times 10^6$ g/m^3 [5], $\Delta\alpha \sim 1$ J/m^2 and $q \sim 2 \times 10^{-19}$ J, $R = (0.1–1.0)T_0/\delta T$ nm at $T_m = 300$ K, we obtain $R \sim 0.1–1.2$ nm, which corresponds to the cluster size d of 2 nm from the Mössbauer spectrum. We also note that the appearance of a peculiar solid–liquid state with a higher atomic mobility can explain the effect of adsorption strength lowering (Rehbinder's effect) [26] on the atomic-molecular level, due to wetting and strain under the action of surfactants.

Mössbauer spectroscopy is unsuitable for systems containing no iron. Therefore, the atomic cluster mobility in nanosystems containing no iron was studied by the method of Rayleigh scattering of Mössbauer radiation, which we elaborated earlier for studying proteins and other biopolymers [27].

We studied the atomic mobility of polymeric networks and of water molecules included in a polymer or a sorbent [11]. The objects for study were (a) SGC-7 acrylate cationite (Institute of Chemical Technology, Russia) on the basis of polyacrylic acid cross-linked with divinyl benzene to the cross-linking degree 2 wt% and (b) Porolas TM polymeric sorbent (Institute of Chemical Technology, Russia) on the basis of the copolymer of divinylbenzene (70%) and ethylstyrene (30%).

The acrylate cationite strongly swells on hydration, which increases the atomic mobility of the polymeric network. Figure 8 represents the data on the Rayleigh scattering of Mössbauer radiation at increasing hydration for SGC-7 (2%). For a dehydrated weakly cross-linked sample, the elastic fraction $f_R = 0.77$ of the Rayleigh scattering of Mössbauer radiation is large enough and characteristic of the polymer in the glassy or crystalline state. The integral value of f_R is dramatically decreased by hydration (Fig. 8a). To determine the hydration dependence of the polymeric network of the cationite in itself, we should take into account the contributions of polymer and water atoms to the integral value of f_R. For a multicomponent system

$$f_R = \frac{\sum_i \left\{ C_i \sum_j \frac{U_j}{A_j} f_{oj}^2 \right\}}{\sum_i \left\{ C_i \sum_j \frac{U_j}{A_j} (f_{oj}^2 + F_j) \right\}}, \qquad (20)$$

where summation over j is carried out over all atoms of the ith component with atomic mass A_j, concentration U_j, atomic scattering factor f_{oj}, and Compton scattering amplitude F_j.

As follows from Fig. 8a, the experimental $f_R(h)$ points lie considerably lower than the integral curve computed with the aid of Eq. (20) under the assumption that $f_R(h)$ in independent of the hydration degree for the polymer and $f_R(H_2O) = 0$ for water in the polymer. Similar results were obtained earlier in investigations on the hydration dependence of the dynamics of biopolymers by the method of Rayleigh scattering of Mössbauer radiation. This means that the elastic fraction of the Rayleigh scattering of Mössbauer radiation of the polymeric network itself decreases on hydration.

From the resulting $f_R(h)$ values one can obtain the rms displacement of atoms, using the equation

$$f_R = a\exp(-Q^2\langle x^2\rangle), \quad (21)$$

where $a = R/(R + C)$, R and C are the intensities of Rayleigh and Compton radiation, respectively, $\langle x^2\rangle$ is the rms displacement of atoms, $Q = 1.53$ Å^{-1} the wave vector of Rayleigh scattering of Mössbauer radiation. As a result, $\langle x^2\rangle = 0.11$ Å^2 ($h = 0$) and $\langle x^2\rangle = 0.91$ Å^2 ($h = 0.66$).

There is quite a different dependence of f_R for the Porolas TM polymeric sorbent (Fig. 8b). This sorbent is hydrophobic. The supramolecular structure of the sorbent is a system of rigidly cross-linked, with mutually penetrating chains, polymeric globules which are 100 nm in size and also possess some internal porosity. By analogy with the cationite, one might expect the operation of the simplest model including a rigid polymeric network, whose intramolecular mobility is independent of hydration because of the intrinsic rigidity of the network and the weak interaction with water [$f_R(h)$ = const], and the free water whose mobility is assumed to be unlimited [$f_R(H_2O) = 0$]. The results of measurements contradict this model. In contrast with the cationite, all the experimental points lie well above the model curve. This makes one to assume $f_R(h) > 0$ at least for a part of water molecules.

It is well known that the Mössbauer effect is absent in liquids of low viscosity because of large (as compared with solids) atomic displacements and strong diffusion broadenings of Mössbauer lines. This also relates to the Rayleigh scattering of Mössbauer radiation. Nevertheless, the Mössbauer effect was observed in liquids located in small pores of a solid [28, 29]. This can be assigned both to the small size (several nanometers) and to the strong interaction of molecules of the liquid with the solid matrix [29]. In this connection, our observation of a low-mobility water in a nanosystem with a weak water–solid interaction is of especial interest.

Much Porolas TM pores are smaller than 3 nm. This size is smaller than in the Vycor porous glass where the Mössbauer effect is observed for liquids [29]. It is very small water clusters in the smallest pores (0.7 g per gram sorbent) which we consider responsible for the elastic fraction of Rayleigh scattering of Mössbauer radiation $f_R(H_2O) > 0$.

It can be assumed that thid result is explained by the small size of the cluster, when decreasing number of vacancies or density fluctuations decrease the rate of self-diffusion of water molecules within the cluster which as a whole is also of low mobility because of the sorbent pore confinement.

b. Intercluster Dynamics

The motion of a cluster as a whole in a nanosystem is a specific field related both to membrane permeability and diffusion in nanosystems and to the low-frequency contribution to thermal properties: heat capacity, heat conduction, etc.

Convenient nanosystems for investigating this motion are ion-exchange cationites, copolymers of styrene and divinylbenzene of various cross-linkage degrees (1%, 2%, and 12%) and with various sets of nanopores, accommodating 3-nm ferric hydroxide clusters [30]. Thus, the nanoclusters are placed in cells whose size varies with cross-linkage degree and which confine diffusion of ferric hydroxide clusters. The Mössbauer spectra of the hydroxide clusters in systems with variable cross-linkage degree are represented in Fig. 9. The spectra (scan rate up to ±100 nm/s) characteristically contain a narrow and a broad components.

The motion of ferric hydroxide clusters can be understood on the basis of the model of restricted diffusion in the field of a certain potential. Moreover, the potential shape and the diffusion rate can be obtained from the temperature dependence of the area of the narrow component and from the shape of the broad component. A Mössbauer spectrum consists of a set of Lorentz components with narrow lines with the intensity

$$A_0 = z^{-2}\left|\int e^{i\vec{k}\vec{R}}e^{-u(R)/k_BT}d^3R\right|^2,$$

$$z = \int e^{-u(R)/T}d^3R,$$

where k is the radiation wave vector and R is the cluster radius. Analysis of the $A_0 = f(T)$ function make possible reconstruction of the motion potential $V(R)$. From the temperature dependence $A_0 = f(T)$ for

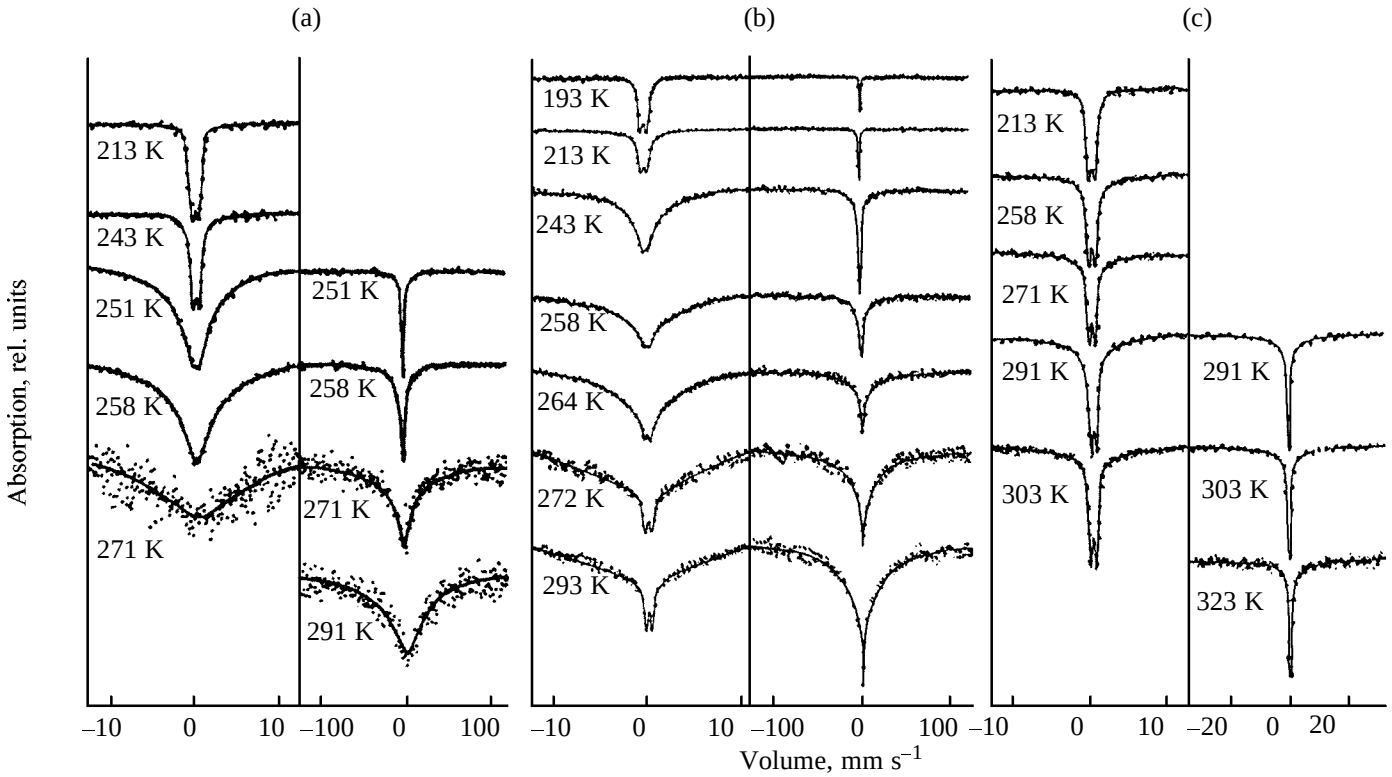

Fig. 9. Mössbauer spectra of ferric hydroxide in the ion-exchane sulfonated resin at various temperatures. Cross-linkage degree, %: (a) 1, (b) 2, and (c) 12.

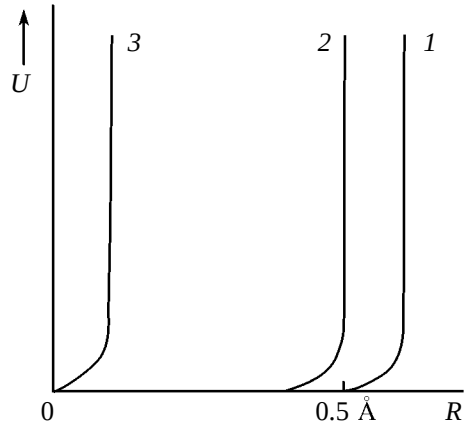

Fig. 10. Shape of potential wells for the motion of ferric hydroxide clusters in the ion-exchange sulfonated resin. Cross-linkage degree, %: (*1*) 1, (*2*) 2, and (*3*) 12.

sample B (2% cross linkage) we have $A_0 = 0.06$ (T = 264–243 K) and the potential shape as a square (spherical) well with elastic walls (Fig. 10). If one assumes that only the diffusion coefficient is temperature-dependent in a spherical cell of radius a, then

$$A_0 = \frac{g(\sin ka - ka\cos ka)^2}{(ka)^6}.$$

For ka = 3.6, the potential well radius a = 0.5 Å. The spectrum calculated with such parameters nicely fits experiment. Increased cell size (sample A) yields a = 0.62 Å, and decreased cell size (sample C) leads to complete restriction of cluster motion by the polymeric network. Thus, the maximum gap between the cluster and network is 0.62 Å. Similar motions with restricted diffusion are observed in ferric oxyhydroxide clusters in the iron-collecting protein ferritin [31].

c. Magnetic Phase Transitions

Similarly to bulk magnetics, isolated nanoclusters and nanosystems feature second-order phase transitions, Langevin magnetization dependences [32], and disappearance of magnetic order and spontaneous magnetization at the Curie temperature T_c or the Neel temperature T_N. In addition, nanosystems can possess superparamagnetism, which leads to effective lowering of T_c and T_N. These transitions are also characterized by smooth temperature dependences of magnetization. However, first-order magnetic phase transitions were observed for a number of clusters of metal oxides, when a nanosystem lost its spontaneous magnetization abruptly at a certain T_{cc} or at a certain critical cluster size (smaller clusters passed to the

paramagnetic, rather than superparamagnetic state). First-order magnetic phase transitions are hardly observable by magnetization measurements, because clusters are scattered in size and T_{cc}. This scatter inevitably leads to smooth changes in magnetization and is hardly distinguished from the superparamagnetic behavior. However, paramagnetic and magnetically ordered states can be distinguished with the aid of Mössbauer spectroscopy. Such jump magnetic phase transitions were observed in nanoclusters and iron oxide nanosystems [1, 6] and explained in terms of first-order magnetic phase transitions. Note that first-order magnetic phase transitions were observed in a number of bulk oxides and alloys of transition and rare-earth metals [32] and interpreted from a thermodynamic standpoint [33].

A thermodynamic model of magnetic phase transitions in nanoclusters was proposed in [6]. Clusters are assumed to possess a strong magnetostriction effect, i.e. they change volume in passing from the magnetically ordered state to paramagnetic. Herewith, the Curie point of a substance depends on its volume:

$$T_c = T_0[(1 + \beta(V - V_0)/V_0], \quad (22)$$

where T_0 is the Curie point of bulk material without changing volume, β is the magnetostriction constant, V and V_0 are the molecular volumes in the magnetically ordered and paramagnetic states, respectively. The change in the free energy density on the transition from the magnetically ordered state to paramagnetic is given by the equation

$$\Delta G_V = -1/2NkTm^2 + 1/2\eta[(V - V_0)/V_0]^2 + 2(\alpha/R)(V - V_0)/V_0 + 1/2NkT[\ln(1 - m^2)/4 + m\ln(1 + m)(1 - m)], \quad (23)$$

where the first term corresponds to the exchange energy density in the molecular field approximation ($m = M/M_s$ is the relative magnetization, M_s is the saturation magnetization); the second term corresponds to the strain energy; the third term is the surface energy (α is the surface tension); and the fourth terms is the entropic term for the temperature dependence of magnetization (N is the number of atoms with spin 1/2, k is Boltzmann's constant, and η is compressibility).

After minimizing the free energy and solving the set of equations $dG_V/dV = 0$ and $dG_V/d_m = 0$, we obtain

$$T/T_{co} = m(1/3\gamma m^2 + 1)\{1/2\ln[1(1 + m)(1 - m)]\}^{-1}, \quad (24)$$

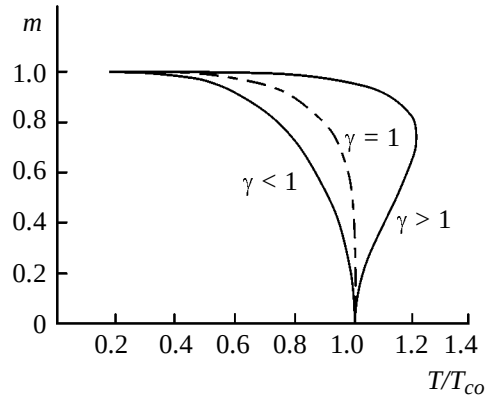

Fig. 11. Cluster magnetization at various γ vs. temperature (see text).

where $\gamma = (3/2)NkT_0\eta\beta^2(1 - \beta\eta P)^{-1}$, and $T_{co} = T_0(1 - \beta\eta P)$ shows changes in T_0 with pressure (cluster surface tension, $P = 2\alpha/R$).

Figure 11 displays the temperature dependence $m = f(T/T_{co})$ for various γ values. The character of a magnetic phase transition is determined by the parameter γ: for a second-order magnetic transition $\gamma < 1$ and for a first-order magnetic transition $\gamma \geq 1$. The descending branch of the temperature dependence corresponds to a maximum of the free energy, i.e. $\gamma \geq 1$. The quantity γ can be represented in the form $\gamma = T_{cc}/T_{co}$ where $T_{cc} = (3/2)NkT_0^2\eta\beta^2$. Thus, at $\gamma \geq 1$, the cluster passes from the magnetically ordered state to paramagnetic via a first-order phase transition if the cluster size

$$R \leq R_{cr} = 2\alpha\beta\eta(1 - T_{cc}/T_{co})^{-1}. \quad (25)$$

For large clusters, there exist only second-order phase transitions that can also show up in supermagnetism at temperatures $kT > KV$.

First- and second-order phase transitions were observed in ferrihydrite $Fe_5HO_8 \cdot 4H_2O$ clusters in polysorb pores [6]. As was already noted, such a system of clusters in pores allows the cluster size to be decreased by decreasing pore size and the initial iron concentration in a pore. Moreover, it makes possible investigation both of a system with isolated clusters and of a system with interacting clusters if there are several clusters in one pore. Figures 12 and 13 show the Mössbauer spectra of ferrihydrite in polysorb pores 13 and 20 nm in size with ^{57}Fe concentrations C of 1.2×10^{-3} and 1.2×10^{-2} M, respectively. As readily seen, the spectra at 4.2 K contain a quadrupole doublet, a central component of the spectrum, and a magnetic hyperfine structure with relatively narrow lines (with account for the dis-

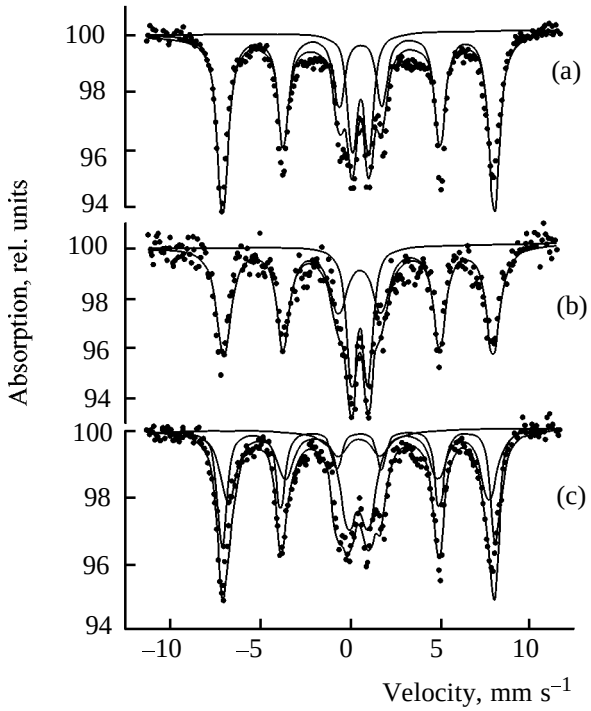

Fig. 12. Mössbauer spectra of ferrihydrite clusters (C = 1.2×10^{-3} M) in polysorbs with the pore size (a, b) 13 and (c) 20 nm. Temperature, K: (a) 4.2, (b) 10, and (c) 4.2.

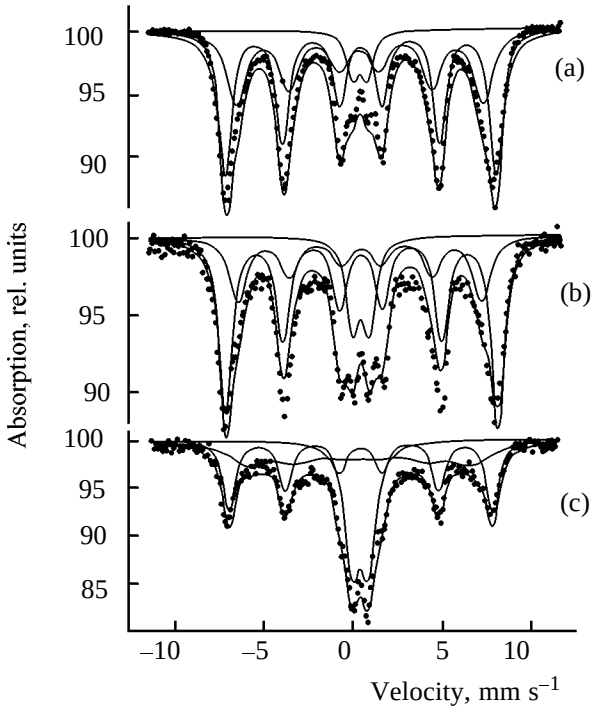

Fig. 13. Mössbauer spectra of ferrihydrite clusters (C = 1.2×10^{-2} M) in polysorbs with the pore size 13 nm. Temperature, K: (a) 4.2, (b) 6, and (c) 10.

ordered cluster structure). As the temperature is increased, a part of the magnetic hyperfine structure of the spectrum changes to a paramagnetic doublet, bypassing intermediate forms associated with superparamagnetism. Increasing iron concentration leads to increasing cluster size. Nevertheless, the spectra at 4.2 and 6 K are similar to each other (Fig. 13), like those at 4.2 and 10 K in Figs. 12b and 12b, i.e. there is a jump transition from the quadrupole doublet to the magnetic hyperfine structure. For a larger cluster size or in the presence of several interacting clusters in the pore of 13 nm at 10 K (Fig. 12c), line broadening is observed, i.e. the presence of intermediate forms, the attributes of superparamagnetism, between the quadrupole doublet and the magnetic hyperfine structure. The results represented in Figs. 12 and 13 allow us to suppose occurrence of a first-order magnetic phase transition (as a jump) in ferrihydrite clusters within the temperature range 4.2–6 K. For smallest clusters (C = 1.2×10^{-3} M), there is practically no line broadening and no evidence for a second-order magnetic transition (the phenomenon of superparamagnetism). For larger clusters at 10 K, in addition to the first-order phase transition, a second-order magnetic transition is observed, accompanied by broadening and shifting of the magnetic hyperfine structure lines due to superparamagnetism. The appearance of superparamagnetism at 10 K allowed estimation of the upper cluster size from the broadening of the magnetic hyperfine structure lines (Fig. 12c), which yielded $R \approx 2$ nm.

The estimation of the cluster size in pores from the data on the iron concentration $C = 1.2 \times 10^{-3}$ M leads to $R \approx 1$–2 nm for an isolated cluster in a pore. Thus, these and superparamagnetic relaxation data yield $R_{cr} \approx 1.5$–2 nm.

Further growth of clusters and strengthening of their interaction are accompanied by appearance of second-order magnetic transitions. The magnetic hyperfine structure lines broaden strongly, which makes the first-order phase transition impossible to distinguish on the background of the second-order phase transition. Estimating the size R_{cr} by Eq. (25) for the critical size using constants yields $R_{cr} \approx 1$, which coincides with experimental results in the order of magnitude.

Effects similar to the first-order magnetic phase transition were also observed in α-Fe_2O_3, α-FeOOH, and γ-Fe_2O_3 nanoclusters and in the proteins ferritin and hemosiderin including the magnetic nucleus $(FeOOH)_8 \cdot (FeOOPO_3H)$ [1].

As was already noted, magnetic phase transitions in a nanocluster system depend on temperature and cluster size. Excess external pressure is one more

parameter determining the character of magnetic phase transition, T_c and R_{cr}. The change in T_c was determined in Eq. (24) as $T_{co} = T_0(1 - \beta\eta P)$, the decrease of the critical temperature of phase transition occurring due to the capillary pressure $P_s = 2\alpha/R$. The change of external pressure P_0 by ΔP changes the temperature of magnetic transition in a cluster by the quantity [8]

$$\Delta T_{co}/T_0 \sim \Delta P(2\alpha/R - 1/\beta\eta)^{-1}. \quad (26)$$

Thus, increasing pressure in a system of nanoclusters should decrease T_{co} and increase the probability of the first-order magnetic phase transition. In [8], two nanosystems were studies, where the interaction of iron hydroxide clusters with a polymeric and biopolymeric network was changed by hydration. The first system was an ion-exchange resin (sulfonated cationite) including ferric hydroxide clusters 3 nm in size. The second system was the globular protein ferritin containing ferric hydroxide clusters 6 nm in size. The excess pressure on a cluster was determined by the strain of the polymeric matrix, produced by the increase in the water volume on crystallization (freezing) and was

$$\Delta P = (1/\eta_m)\Delta V/V. \quad (27)$$

At $\Delta V/V = 0.09$ for water and $1/\eta_m$ = (5–10) GPa [8], the estimation yields ΔP = (0.45–0.9) GPa, which is comparable, by magnitude, with the capillary pressure in a 1.5-nm cluster (~1 GPa). The pressure-induced decrease in T_{co} can be estimated by Eq. (27). Setting $P = 2\alpha/R$ ~1 GPa, $\beta = 10^2$, $\eta = 10^{-11}$ m^2/J, and $1/N$ ~10–28 m^3, we obtain $\Delta T_{co} = (0.1–1.0)T_{co}$. Thus, the decrease ΔT_{co} can attain the order of magnitude of the quantity T_{co} itself.

The ΔT_{co} value can be estimated from the Mössbauer spectra of the sulfonated cationite in the range T = 4.2– 30 K and of ferritin in the range 4.2–78 K [8]. It was shown that hydration with subsequent freezing decreased T_{co} which was determined at the equality of the paramagnetic part and the magnetic hyperfine structure of the spectra. The following quantities were determined: $T_{co} \approx$ 9–10 K for hydrated sulfonated cationite, $T_{co} \approx$ 13–14 K for dry sulfonated cationite, $T_{co} \approx$ 30 K for hydrated ferritin, and $T_{co} \approx$ 30–34 K for dry ferritin. Comparison of the T_{co} values yields the temperature shift $\Delta T_{co} \approx$ 3–4 K, which agrees with thermodynamic estimates.

First-order magnetic phase transitions stimulated by intercluster stresses and defects also arise in nanosystems with larger nanoclusters (20–50 nm), obtained by solid-phase chemical reactions [9]. Significant intercluster interactions arise in the process of cluster sintering because of the development of a large defect density and of heterogeneity of the system with different volumes of elementary cells, for example, of γ-Fe_2O_3 with the spinel structure and α-Fe_2O_3 with the corundum structure. In such nanosystems, first-order magnetic phase transitions were observed, as well in ferrihydrite clusters 1–3 nm in size in the polymeric matrix. Figure 14 represents the Mössbauer spectra of the α–γ-Fe_2O_3 nanosystem, characterizing jump magnetic transitions from the magnetically ordered state (magnetic hyperfine structure) to the paramagnetic state (central doublet). These magnetic transitions proceed at lower (as compared with bulk α- and γ-Fe_2O_3, T_0 = 856 and T_0 = 965 K, respectively) critical points T_{co} = 120–300 K. The decrease in T_{co} cannot be a consequence of superparamagnetism because of large dimensions of clusters, so that the calculation leads to relaxation times several orders larger than τ_{exp}. As a result, magnetization B_{in} ~50 t disappears abruptly to B_{in} ~0, which is associated with the transformation of the magnetic hyperfine structure of γ-Fe_2O_3 into a paramagnetic doublet (Fig. 13) and characterizes a first-order phase transition.

The reasons for this phenomenon in such a nanosystem are related to strong intercluster interactions leading to significant stresses in the nanosystem. These stresses stimulate pressures up to several gigapascals, which develop on sintering [14] of elementary cells of α- and γ-Fe_2O_3 with different volumes and under the action of defects and dislocations. As was shown earlier [34, 35], the density of defects can be a maximum just at the size 20–30 nm. This induces stresses and jump magnetic phase transitions with lowering T_{co} values characteristic for a certain cluster size. Further increase in cluster size decreases the fraction of interfaces and the defect density, so that the cluster properties approach the characteristics of bulk matter. Magnetic phase transitions and decrease in T_c in clusters were proposed to describe in terms of the following model. If n_0 is the initial number of defects in a cluster and n_c is the number of defects passing in the intercluster space, we have

$$n_0 = n_v + n_s = c_0 N_s = \text{const},$$

where n_v is the number of defects remaining in the cluster and N_s is the number of atoms in the intercluster space. Assuming that the magnetic phase transition temperature T_c decreases with increasing concentration of cluster defects $c_v = n_v/N_v$ (N_v is the number of atoms in the cluster) and the dependence is linear at small c_v at the temperature T_{co} of a defectless cluster, we obtain

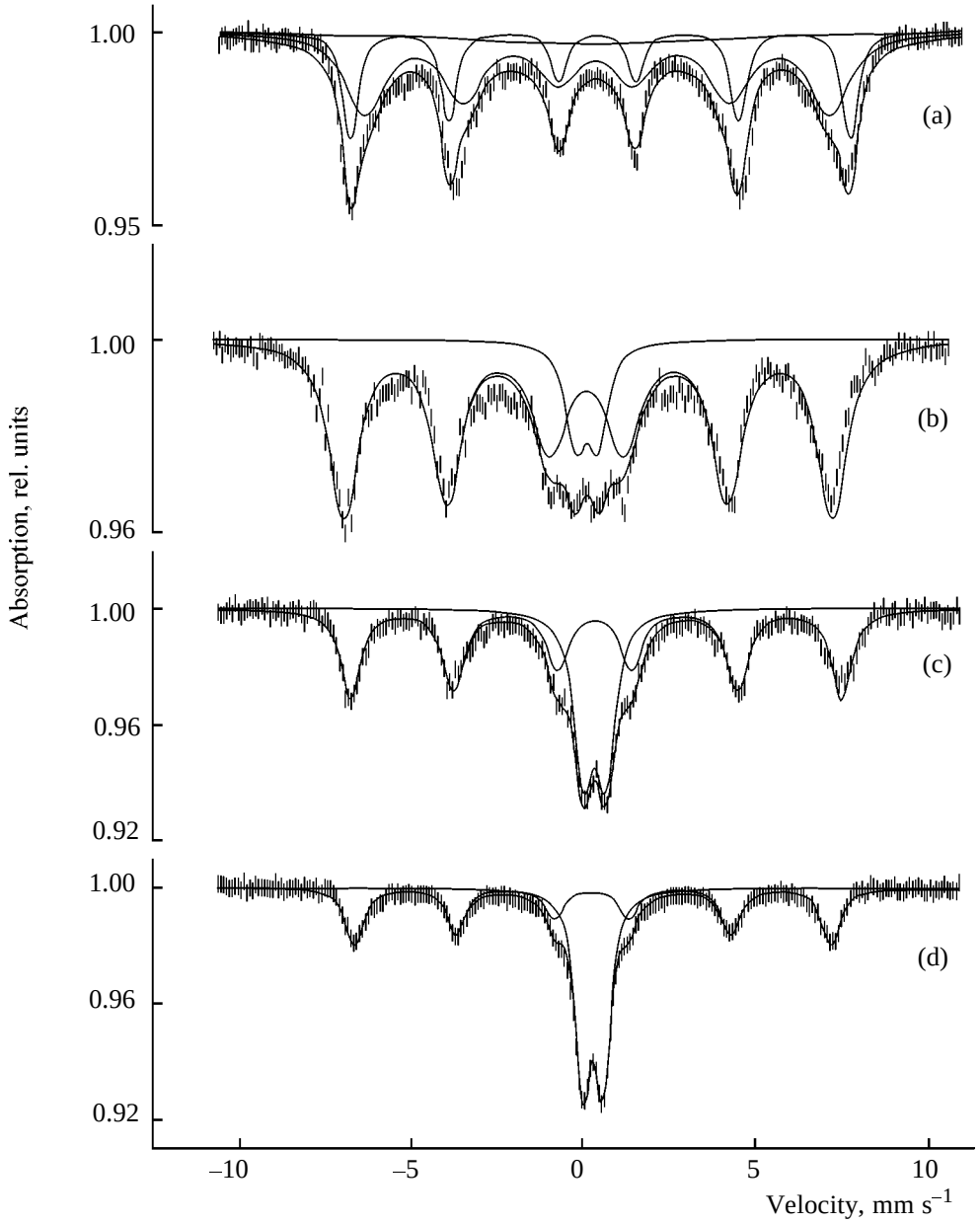

Fig. 14. Mössbauer spectra of the α-Fe_2O_3–γ-Fe_2O_3 nanosystem at various temperatures. Temperature, K: (a) 77, (b) 120, (c) 160, and (d) 300. (Solid lines) Results of computer deconvolution of the spectra.

$$T_c = T_{co}(1 + \beta c_v),$$

where $\beta < 0$ is a constant. Accounting for magnetization m, the thermodynamic potential of a system can be expressed as

$$G = \Delta\mu n_v + \alpha S(n_v) - (1/2)N_v kT_{cR}(1 + \beta a_v)m^2 + NkT\{(1/2)\ln[(1 - m^2)/4] + m\ln[(1 + m)/(1 - m)]\}, \quad (28)$$

where $\Delta\mu = \Delta\mu_o + kT\ln(N_s n_v/N_v n_s)$ is the difference of the chemical potentials of defects inside and outside the cluster, α is the surface tension of the cluster, S is the cluster surface, N is the number of spins in the cluster, and m is the magnetic moment of the system. Dividing the cluster volume $V = N_v w + n_v v$ and accounting for the atomic volume w and the defect volume v, we obtain $v dn_v = dV$. In consideration of $dS/dV = 2/R$ for a sphere, we obtain $dS/dn_v = v dS/dV = 2v/R$. If the conditions $dG/dn = 0$ and $dG/dm = 0$ are fulfilled simultaneously, Eq. (28) can be reduced to the form

$$1 + (\beta c_o)q(R)/\{1 + q(R)K\exp[(v dp(R)/kT_{co} - 5(u\beta)m^2)(T_{co}/T)]\} - [(1/2)/m]\ln[(1 + m)/(1 - m)]T/T_{co}) = 0, \quad (29)$$

where $q(R) = [(1 + r/R)^3 - 1] = [(1 + (r/a)(a/R))^3 - 1]$, $dp(R) = 2\alpha/R$, and $u = N/N_v$ is the spin number concentration in the cluster, a is the lattice constant, r is the thickness of intercluster space. At calculating the magnetization curve $m(T/T_{co})$, we used the following parameters: (1) βc_o; (2) $K = \exp(-\Delta\mu_0/kT_{co})$; (3) $u\beta$; (4) r/a; (5) $2\alpha v/a/kT_{co}$. Figure 15 represents the dependence of magnetization m on T/T_{co} for clusters with R ranging from $500a$ to $3a$. From the curve with the parameters $\beta c_o = -50$, $K = 0.01$, $u\beta = -3$, $r/a = 1$, $2\alpha v/akT_{co} = 50$ we can see that the dependence of magnetic phase transition on cluster radius changes from a smooth curve characteristic of a second-order phase transition to a jump transition. Along with the first-order magnetic phase transition (Figs. 14a and 16a), two more phase transitions were observed in this nanosystem: a weak ferromagnetic–antiferromagnetic transition and a collective magnetic phase transition with formation of twin nanostructures.

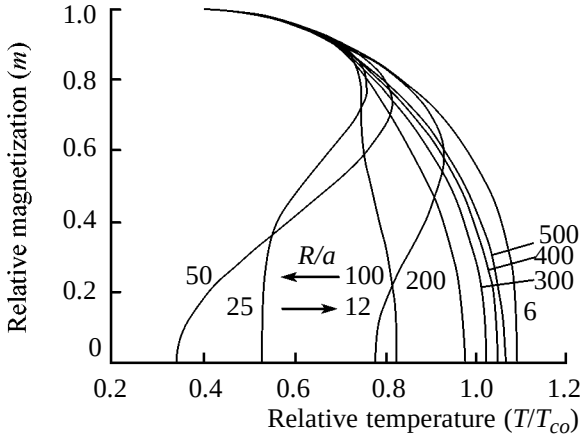

Fig. 15. Nanosystem magnetization calculated with account for defect density at various R/a values vs. temperature.

Magnetic phase transitions like weak ferromagnetism (noncollinear antiferromagnetism)–antiferromagnetism (collinear antiferromagnetism) were observed in α-Fe_2O_3 crystals. Weak antiferromagnetism was also observed for $MnCO_3$, $CoCO_3$, MnF_2, and for trimetric crystals with the structure of rare-earth ferrites $MeFeO_3$ (Me is a rare-earth element) [32]. This effect is related to the state of a ferromagnetic with a certain small degree of noncollinearity of sublattice magnetization. The sublattice magnetization noncollinearity of antiferromagnetic structure was calculated on the basis of the influence of weak magnetic interactions and appeared with increasing temperature as a consequence of instability of equilibrated antiferromagnetism. As was already noted, the nanosystem contains the phase of α-Fe_2O_3 possessing the spinel-type cubic structure and the phase of γ-Fe_2O_3 with the structure of corundum possessing a rhombohedral lattice. For bulk α-Fe_2O_3, there is a magnetic phase transition, also known as the Morin transition, at $T_M \approx 260$ K, when matter changes its type of magnetic ordering by jump. So there is collinear antiferromagnetism at $T_M < 260$ K and noncollinear antiferromagnetism (weak ferromagnetism) at $T_M > 260$ K. This transition is caused by the type of internal symmetry of the crystal, which admits distortions at increasing temperature, accompanied by spin turning by 90°. In Mössbauer spectroscopy, the collinearity–noncollinearity phase transition of sublattice magnetic moments is traced by the change in the sign and magnitude of quadrupole splitting in a spectrum possessing magnetic hyperfine structure:

$$\Delta E_Q = (1/8)e^2qQ(3\cos^2\theta - 1),$$

where q is the electric field gradient, Q is the quadrupole moment of the ^{57}Fe nucleus, θ is the angle between the direction of atomic spin and the direction of the electric field gradient on the nucleus, e is the electron charge. The high-temperature phase of α-Fe_2O_3 corresponds to $\Delta EQ = +0.2$ mm/s and the low-temperature phase, to $E_Q = -0.3$ mm/s. We now consider the specificity of this phase transition. For the nanosystem (Fig. 16b), the low-temperature phase of α-Fe_2O_3 with the parameter $\Delta E_Q = -0.3$ mm/s corresponds to collinear antiferromagnetism. The transition to the state of noncollinear antiferromagnetism with $\Delta E_Q = 0$–0.1 mm/s occurs above $T = 120$ K. As a result, the Morin transition temperature decreases to $T_M \approx 120$ K, the high-temperature phase having a lower ΔE_Q value.

Thus, nanosystems including α-Fe_2O_3 nanoclusters feature jump first-order phase transitions from collinear ferromagnetic to noncollinear antiferromagnetic (possessing weak antiferromagnetism). The decrease in T_M is related to the proportion between the magnetic dipole energy E_M and the exchange energy E_{ex}. The latter decreases with cluster size because of decreased T_{co} for Fe_2O_3. This circumstance increases the probability of existence of noncollinear antiferromagnetism. As a result, the Morin transition occurs already at $T_M = 120$ K.

Noteworthy is one more important feature of the Morin transition in the nanosystems. In spite of the wide size distribution of clusters, the phase transition occurs at a fixed temperature $T_M \sim 120$ K. This gives evidence for collective transformation of the whole nanosystem, when the phase transition in a single cluster initiates the phase transition of the whole sample. Similar phase transitions with instantaneous

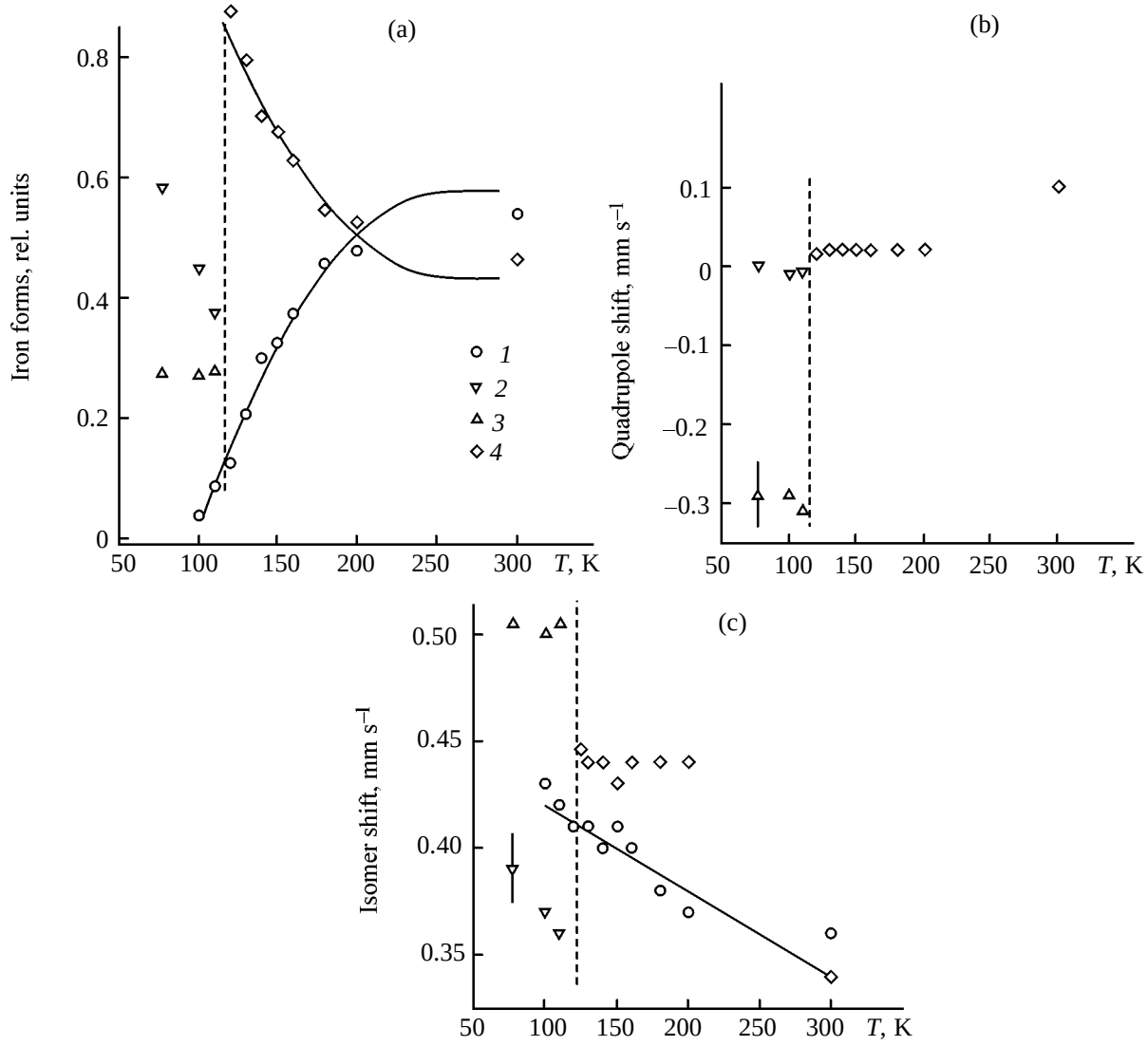

Fig. 16. Results of computer simulation of the Mössbauer spectra of the α-Fe_2O_3–γ-Fe_2O_3 nanosystem: temperature dependences of (a) spectral areas for different forms of iron, (b) quadrupole shift ΔE_Q of magnetic hyperfine structure, and (c) isomer shift. (*1*) Paramagnetic component (quadrupole doublet), (*2*) magnetic component of γ-Fe_2O_3, (*3*) magnetic component of α-Fe_2O_3, and (*4*) component corresponding to the twin structure. The dashed line shows the region of the Morin phase transition.

collective phase transformations of the whole sample were observed in austenite–martensite transitions in carbon steels (martensite transitions) [36].

In α-Fe_2O_3 nanosystems, a general regularity of the temperature behavior of the α- and γ-Fe_2O_3 phases was revealed by Mössbauer spectroscopy. The presence of the two phases, α-Fe_2O_3 and γ-Fe_2O_3, is observed at low temperatures. Above T = 120 K, α-Fe_2O_3 and γ-Fe_2O_3 convert in a single common structure similar, in terms of the parameter ΔE_α, to the α phase but preserving the X-ray diffraction structures of the α and γ phases. The temperature dependence of the isomeric shift (Fig. 16c) points to a dramatic change in δ at T = 120 K. As a result, δ for the α phase decreases and for the γ phase increases jumpwise to the average value δ = 0.45 mm/s. These data suggest the collective transformation of the α and γ phases into an α-like phase with preserved cubic spinel symmetry. This effect can be explained by assuming formation of a twin nanostructure. The phenomenon of twinning is known for crystallization processes at mechanical strains and for sintering of nuclei. Twinning occurs on fast thermal expansion or contraction and on heating of strained crystals [1].

In the course of formation of the nanosystem, there was sintering of iron oxides nuclei with subsequent fast cooling, which led to formation of strongly interacting clusters. This interaction produces stresses and pressures in clusters and causes magnetic phase transitions. Probably, similar interactions give rise to twin collective transitions in the nanosystem.

Thus, twin transitions in the nanosystem are responsible for a specific temperature phase transition. The nanoheterogeneous α–γ system of ferric oxides changes to a one-phase, according to the Mössbauer spectral data, twin structure where the α phase redevelops similarly to the γ phase with electron transfer to the α phase (then the isomer shift increases). Such transition seems to be a new property of a heterogeneous nanosystem where a cluster possessing a collinear first-order phase transition and a collinear–noncollinear antiferromagnetic transition with spin turning by 90° (Morin transition) acts as transition generator and causes collective transition to a twin nanostructure. Indeed, the temperature of twinning phase transition T_t = 120 K for the nanosystem coincides with the temperature of the antiferromagnetic–weak ferromagnetic transition T_M = 120 K. As a result, the collective Morin transition (which is very sensitive to defects in bulk material) initiates the new-type phase transition.

d. Catalytic Properties

The catalytic properties of a nanosystem are determined by the surface state of a cluster, by the cluster size, and by interaction of the cluster with a matrix.

Clusters in carbon and oxide matrices were investigated. Clusters of iron oxide and metallic iron 3–10 nm in size were prepared by thermal decomposition of ferric oxalate with subsequent reduction in a charcoal matrix [7]. Such nanosystems are used for directed transportation of medicinals in the body. For this reason, of interest are systems containing nanoclusters with as-high-as-possible magnetic moment and high adsorption capacity.

In the process of thermal decomposition in a hydrogen atmosphere, the pore size and the carbon adsorptivity sharply increased as functions of the iron content and the cluster size in the process of catalytic hydrogenation of the carbon matrix. This effect is related to burning-out of carbon pores and senhancement of cluster–matrix interaction initiated by hydrogen chemisorption.

The structure–function relationship for catalysts was studied on iron-containing cluster catalysts of oxidative decomposition of hydrogen sulfide on carbon carriers [13]. It was established that the clusters of nonstoichiometric magnetite and pyrrhotine are active structures on the oxidative decomposition of hydrogen sulfide. The activity of magnetite clusters is associated to the presence on the surface of a terminal (not bridging) lattice oxygen, oxygen vacancies, and labile forms of atomic oxygen. The appearance of Fe–S sulfide fragments on the spinel surface points to dissociative adsorption of hydrogen sulfide on anionic vacancies with deposition of elemental sulfur in near-surface cluster layers. The high activity and stability of catalysts on the microporous carrier are probably caused by the presence of relatively large clusters of nonstoichiometric magnetite, 5–10 nm in size, incapsulated in pore mouths. As the cluster size decreases, the mobility of the terminal oxygen and the net activity decrease.

For two Co–Mo–Bi–Fe–Sb–K–O nanocrystalline catalysts differing by the way of introduction of antimony and potassium, the mobility of lattice oxygen in the reaction of partial oxidation of propylene to acrolein was studied [12]. The amount of lattice oxygen participating in the elementary stages of the reaction was determined by two independent methods: from the yield of oxygen-containing products of the oxidation of propylene with the catalyst oxygen in the pulse mode and with the aid of Mössbauer spectroscopy. The agreement of the resulting data shows that the active oxygen of the catalyst lattice is formed by redox transformations of ferric molybdate entering into the composition of the catalysts. The diffusion rate constants for the lattice oxygen were estimated within the frames of the diffusion model. It was shown that increasing oxygen mobility leads to increasing net catalyst productivity and decreasing selectivity of the oxidation process.

ACKNOWLEDGMENTS

The work was financially supported by the Russian Foundation for Basic Research (project no. 00-03-32 267).

REFERENCES

1. Suzdalev, I.P., *Usp. Khim.*, 2001, vol. 70, no. 3, p. 203.
2. Suzdalev, I.P., Buravtsev, V.N., Imshennik, V.K, and Novichikhin, S.V., *Khim. Fiz.*, 1993, vol. 12, no. 4, p. 455.
3. Suzdalev, I.P. and Shklovskaya, N.I., *Colloid Surf. A*, 1996, vol. 108, p. 315.
4. Suzdalev, I.P, Imshennik, V.K, and Novichikhin, S.V.,

Nucl. Instrum. Methods, Phys. Res. B, 1993, vol. 76, p. 421.

5. Suzdalev, I.P., Buravtsev, V.N., Imshennik, V.K., Maksimov, Yu.V., Matveev, V.V., Volynskaya, A.V., Trautwein, A.X., and Winkler, H., *Z. Phys. D*, 1996, vol. 36, p. 163.
6. Suzdalev, I.P., Buravtsev, V.N., Imshennik, V.K., Maksimov, Yu.V., Matveev, V.V., Novichikhin, S.V., Trautwein, A.X., and Winkler, H., *Z. Phys. D*, 1996, vol. 37, p. 55.
7. Imshennik, V.K., Suzdalev, I.P., Stavinskaya, O.N., Shklovskaya, N.I., Schunemann, V., Trautwein, A.X., and Winkler, H., *Microporous Mater.*, 1997, vol. 10, p. 225.
8. Suzdalev, I.P., Plachinda, A.S., Buravtsev, V.N., Maksimov, Yu.V., Reiman, S.I., Khromov, V.I., and Dmitriev, D.A., *Khim. Fiz.*, 1998, vol. 17, no. 2, p. 145.
9. Suzdalev, I.P., Maksimov, Yu.V., Novichikhin, S.V., Buravtsev, V.N., and Imshennik, V.K., *Khim. Fiz.*, 2000, vol. 19, no. 2, p. 105.
10. Suzdalev, I.P., Suzdalev, I.P., Novichikhin, S.V., Buravtsev, V.N., Imshennik, V.K., and Kazakevich, I.P., *Kolloid. Zh.*, 2000, vol. 62, no. 2, p. 257.
11. Plachinda, A.S., Suzdalev, I.P., Kuznetsov, I.A., Baldokhin, Yu.V., and Khromov, V.I., *Izv. Ross. Akad. Nauk, Ser. Khim.*, 1998, no. 10, p. 1996.
12. Firsova, A.A., Maksimov, Yu.V., Bychkov, V.Yu., Isaev, O.V., Suzdalev, I.P., and Korchak, V.N., *Kinet. Katal.*, 2000, vol. 41, no. 1, p. 131.
13. Maksimov, Yu.V., Tsodikov, M.V., Perederii, M.A., Bukhtenko, O.V., Suzdalev, I.P., and Navio, J.A., *Surf. Interf. Anal.*, 2000, vol. 30, no. 1, p. 74.
14. Geguzin, Ya.E., *Fisika spekaniya* (Physics of Sintering), Moscow: Nauka, 1984.
15. Rusanov, A.I., *Usp. Khim.*, 1964, vol. 33, no. 8, p. 873.
16. Rusanov, A.I., *Fazovye ravnovesiya i poverkhnostnye yavleniya* (Phase Equilibria and Surface Phenomena), Leningrad: Khimiya, 1967; German Edition: Phasengleichgewichte und Grenzflachenerscheinungen, Berlin: Akademie, 1976.
17. Hill, T., *Thermodynamics of Small Systems*, New York: Benjamin, 1964, p. 25.
18. Adamson, A.W., *Physical Chemistry of Surface*, New York: Wiley, 1976.
19. Oxtoby, D.W., *Advances in Chemical Physics*, New York: Wiley, 1988, vol. 70, p. 263.
20. Stravinskaya, O.N., Imshennik, V.K., Oranskaya, E.I., Suzdalev, I.P., and Shklovskaya, N.I., *Zh. Fiz. Khim.*, 1998, vol. 72, no. 7, p. 1269.
21. Stravinskaya, O.N., Imshennik, V.K., Novichikhin, S.V., Suzdalev, I.P., and Shklovskaya, N.I., *Zh. Fiz. Khim.*, 1998, vol. 72, no. 7, p. 1282.
22. Lynden, P.M. and Wales, D.J., *J. Chem. Phys.*, 1994, vol. 101, no. 2, p. 1460.
23. Clevend, Ch., Landman, V., and Luedke, W., *J. Phys. Chem.*, 1994, vol. 98, no. 25, p. 6272.
24. Landau, L.D. and Lifshitz, E.M., *Statistical Physics*, Oxford: Pergamon, 1960.
25. Suzdalev, I.P., *Dinamicheskie effekty v gamma-rezonansnoi spektroskopii* (Dynamic Effects in Gamma-Resonance Spectroscopy), Moscow: Atomizdat, 1979.
26. Rehbinder, P.A., *Poverkhnostnye yavleniya v dispersnykh sistemakh. Fiziko-khimicheskaya mekhanika* (Surface Phenomena in Disperse Systems. Physicochemical Mechanics), Moscow: Nauka, 1979, p. 142.
27. Suzdalev, I.P., *Gamma-rezonansnaya spektroskopiya belkov i model'nykh soedinenii* (Gamma Resonance Spectroscopy of Proteins and Model Compounds), Moscow: Nauka, 1988.
28. Burger, K. and Vertes, A., *Nature*, 1983, vol. 306, no. 5941, p. 353.
29. Hietaniemi, J., Ikonen, E., and Katila, T., *Eur. Lett.*, 1992, vol. 18, p. 373
30. Plachinda, A.S., Sedov, V.E., Khromov, V.I., Suzdalev, I.P., Goldanskii, V.I., Nienhaus, G.U., and Parak, F., *Phys. Rev. B*, 1991, vol. 45, no. 14, p. 7716.
31. Bell, S.H., Meir, H.P., Dickson, D.P.E., Gibson, J.P., Sharp. G.A., and Peters, T.V., *Biochim. Biophys. Acta*, 1984, vol. 787, p. 227.
32. Vonsovskii, S.V., *Magnetizm* (Magnetism), Moscow: Nauka, 1971.
33. Bean, C.V. and Rodbell, D.S., *Phys. Rev.*, 1962, vol. 126, no. 1, p. 104.
34. Suzdalev, I.P., Buravtsev, V.N., Imshennik, V.K., Maksimov, Yu.V., and Matveev, V.V., *Izv. Ross. Akad. Nauk, Ser. Fiz.*, 2001, no. 7, p. 1028.
35. Suzdalev, I.P., Buravtsev, V.N., Imshennik, V.K., and Maksimov, Yu.V., *Scripta Mater.*, 2001, vol. 44, no. 8/9, p. 1937.
36. Schulze, G.E.R., *Metall Physik*, Berlin: Academie, 1967.